Author(s): Auvinen, Jussi; Eskola, Kari J.; Huovinen, Pasi; Niemi, Harri; Paatelainen, Risto; Petreczky, Peter

Title: Temperature dependence of η/s : uncertainties from the equation of state

Year: 2019

Version: Published version

Please cite the original version:

Auvinen, J., Eskola, K. J., Huovinen, P., Niemi, H., Paatelainen, R., & Petreczky, P. (2019). Temperature dependence of η/s : uncertainties from the equation of state. In Confinement 2018 : Proceedings of the XIII Quark Confinement and the Hadron Spectrum Conference (Article 135). Sissa Medialab srl. POS Proceedings of Science, 336. https://doi.org/10.22323/1.336.0135

PROCEEDINGS OF SCIENCE

Temperature dependence of η/s: uncertainties from the equation of state

Jussi Auvinen[*,a], **Kari J. Eskola**,[b,c] **Pasi Huovinen**,[d] **Harri Niemi**,[b,c] **Risto Paatelainen**[e] **and Péter Petreczky**[f]

[a] *Institute of Physics Belgrade*
Belgrade, Serbia
[b] *University of Jyväskylä*
Department of Physics
P.O. Box 35, FI-40014 University of Jyväskylä, Finland
[c] *Helsinki Institute of Physics*
P.O. Box 64, FI-00014 University of Helsinki, Finland
[d] *University of Wrocław*
Wrocław, Poland
[e] *CERN*
Geneva, Switzerland
[f] *Physics Department*
Brookhaven National Laboratory
Upton, NY 11973. USA

E-mail: auvinen@ipb.ac.rs

We perform a global model-to-data comparison on Au+Au collisions at $\sqrt{s_{NN}} = 200$ GeV and Pb+Pb collisions at 2.76 TeV and 5.02 TeV, using a 2+1D hydrodynamics model with the EKRT initial state and a shear viscosity over entropy density ratio $(\eta/s)(T)$ with a linear T dependence. To quantify the amount of uncertainty due to the choice of the equation of state (EoS), we compare analysis results based on four different EoSs: the well known $s95p$ parametrisation, an updated parametrisation based on the same list of particles in hadron resonance gas, but using recent lattice results for the partonic part of the EoS, and two new parametrisations based on the Particle Data Group 2016 particle list and the recent lattice results. We find that the choice of the EoS does affect the favoured minimum value of η/s, although within the confidence limits of the analysis. On the other hand, our analysis hardly constrains the temperature dependence of η/s, no matter the EoS.

XIII Quark Confinement and the Hadron Spectrum - Confinement2018
31 July - 6 August 2018
Maynooth University, Ireland

*Speaker.

PoS(Confinement2018)135

1. Introduction

Recent advancements in multi-parameter model-to-data comparison have provided notable constraints on the minimum value and temperature dependence of the shear viscosity over entropy density ratio, η/s, of the matter produced in the heavy-ion collisions at RHIC and the LHC. The results of a Bayesian analysis with a flexible initial state parametrisation [1, 2] agree with the temperature dependence of η/s found in the earlier study using the EKRT pQCD + saturation + hydrodynamics model [3].

However, with the exception of papers like Refs. [4, 5, 6], the equation of state is taken as given in models used to extract the η/s value from the data. Furthermore, in many studies in the literature, EoS parametrisation $s95p$ [7] was used, a parametrisation which is based on by now outdated lattice data [8]. To find out whether the works employing the $s95p$ parametrisation are still relevant, and whether the present uncertainties in the lattice results affect the value of η/s extracted from the data, we perform a Bayesian statistics based analysis using four different parametrisations of EoS. We compare the data obtained in $\sqrt{s_{NN}} = 200$ GeV Au+Au collisions [9, 10] and Pb+Pb collisions at 2.76 TeV [11, 12] and 5.02 TeV [12, 13] to the results of EKRT + hydrodynamics calculations [3, 14] with a linear parametric form for $(\eta/s)(T)$. The resulting probability distributions for the best-fit parameters indicate not only whether the most probable parameter values depend on the EoS used, but also whether the difference is larger than the overall uncertainty in the fitting procedure.

The structure of this proceedings article is the following: we describe the main features of the hydrodynamics model and the equations of state in Section 2. A summary of the statistical analysis methods is given in Section 3. The results are presented in Section 4 and summary in Section 5.

2. Hydrodynamical model and the equations of state

We use a viscous 2+1D hydrodynamical model [3] with a linear parametrisation of the temperature dependence of η/s:

$$(\eta/s)(T) = \begin{cases} S_{HG}(T_{min} - T) + (\eta/s)_{min}, & T < T_{min} \\ S_{QGP}(T - T_{min}) + (\eta/s)_{min}, & T > T_{min}, \end{cases} \tag{2.1}$$

where the free parameters are the minimum value of shear viscosity over entropy density ratio $(\eta/s)_{min}$, the location of the minimum in temperature T_{min}, and the slopes below and above T_{min}, denoted by S_{HG} and S_{QGP}, respectively.

The initial energy density distribution is determined using the event-averaged EKRT minijet local saturation model [15, 16]:

$$e(\vec{r}_T, \tau_s(\vec{r}_T)) = \frac{K_{sat}}{\pi}[p_{sat}(\vec{r}_T, K_{sat})]^4, \tag{2.2}$$

where $p_{sat}(\vec{r}_T, K_{sat})$ is the local saturation scale, $\tau_s(\vec{r}_T) = 1/p_{sat}(\vec{r}_T, K_{sat})$ is the local formation time, and the proportionality constant K_{sat} is one of the free parameters of our model.

We utilise four different parametrisations of EoS, which all combine hadron resonance gas at lower temperatures with lattice QCD at high temperatures. We prefer to not use the lattice data

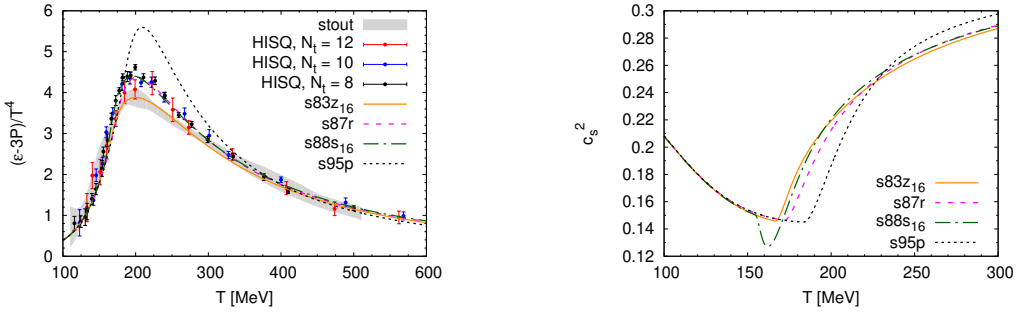

Figure 1: Left panel: The trace anomaly as a function of temperature in the four parametrisations of the EoS compared to the lattice data obtained using HISQ [18, 19] and stout [21] discretisation schemes. Right panel: The speed of sound squared as function of temperature in the four parametrisations of the EoS.

to parametrise the EoS below $T = 155$ MeV temperature to allow energy and momentum conserving particlization without any non-physical discontinuities in temperature and/or flow velocity. Our baseline is the well-known $s95p$ parametrisation [7] where hadron resonance gas containing hadrons and resonances below $M < 2$ GeV mass from the 2005 PDG summary tables [17] is connected to parametrised hotQCD data from Ref. [8].

To gauge the effect of various developments during the last decade, we first connect the hadron resonance gas of PDG 2005 particle list [17] to parametrised set of contemporary lattice data obtained using the HISQ discretisation scheme [18, 19]. To follow the convention used to name $s95p$, we label this parametrisation $s87r$ since entropy density reaches 87% of its Stefan-Boltzmann value at $T = 800$ MeV. The number of well-established resonances has increased since 2005, and thus we build our parametrisation $s88s_{16}$ based on hadron gas containing all strange and non-strange hadrons and resonances in PDG 2016 summary tables[1] [20], and on contemporary HISQ lattice data [18, 19]. Furthermore there is slight tension in the trace anomaly between the HISQ and stout discretisation schemes, and to explore whether this difference has any effect on hydrodynamical modeling, we base our $s83z_{16}$ parametrisation on PDG 2016 resonances, and the continuum extrapolated lattice data obtained using the stout discretisation [21]. To characterise the differences in the parametrisations, we show the trace anomaly and the speed of sound squared as a function of temperature in Fig. 1.

In all the calculations presented here, the kinetic and chemical freeze-out temperatures are $T_{\rm dec} = 150$ MeV, and bulk viscosity is taken to be zero.

3. Statistical analysis

Our model has five free parameters $\{K_{sat}, T_{min}, (\eta/s)_{min}, S_{HG}, S_{QGP}\}$ which need to be fixed by looking for the best reproduction of experimental data. Representing a point in the input parameter space with $\vec{x}$, a corresponding point in the output (observable) space with $\vec{y}(\vec{x})$, and the experimental data with $\vec{y}^{\rm exp}$, we can determine the posterior probability distribution $P(\vec{x}|\vec{y}^{\rm exp})$ of the best-fit parameter values by utilising Bayes' theorem:

$$P(\vec{x}|\vec{y}^{\rm exp}) \propto P(\vec{y}^{\rm exp}|\vec{x})P(\vec{x}), \tag{3.1}$$

[1] Subscript "16" in the label of the parametrisation refers to the use of the PDG 2016 list.

where $P(\vec{x})$ is the prior probability distribution of input parameters and $P(\vec{y}^{\,\mathrm{exp}}|\vec{x})$ is the likelihood function

$$P(\vec{y}^{\,\mathrm{exp}}|\vec{x}) = \frac{1}{\sqrt{|2\pi\Sigma|}} \exp\left(-\frac{1}{2}(\vec{y}(\vec{x}) - \vec{y}^{\,\mathrm{exp}})^T \Sigma^{-1} (\vec{y}(\vec{x}) - \vec{y}^{\,\mathrm{exp}})\right), \tag{3.2}$$

in which Σ is the covariance matrix representing the uncertainties related to the model-to-data comparison.

We produce samples of the posterior probability distribution with Markov chain Monte Carlo (MCMC) [22], by initialising an ensemble of random walkers in the input parameter space based on the prior probability, and accepting or rejecting each proposed step based on the likelihood function. The distribution of the taken steps then converges to the posterior distribution at a large number of steps.

However, as we want to have an ensemble of $\mathcal{O}(100)$ walkers performing $\mathcal{O}(1000)$ steps, it becomes infeasible to compute the likelihood function by running the full hydrodynamics simulation for each random input parameter combination $\vec{x}$. Instead, we utilise Gaussian process (GP) emulators [23] as a surrogate model, and our likelihood function becomes

$$P(\vec{y}^{\,\mathrm{exp}}|\vec{x}) = \frac{1}{\sqrt{|2\pi\Sigma|}} \exp\left(-\frac{1}{2}(\vec{y}_{GP}(\vec{x}) - \vec{y}^{\,\mathrm{exp}})^T \Sigma^{-1} (\vec{y}_{GP}(\vec{x}) - \vec{y}^{\,\mathrm{exp}})\right), \tag{3.3}$$

where $\vec{y}_{GP}(\vec{x})$ represents the GP estimate of the model output. In this case, the covariance matrix includes also the emulator estimation error

$$\Sigma = \mathrm{diag}((\sigma_{\mathrm{exp}})^2 + (\sigma_{\mathrm{GP}}(\vec{x}))^2), \tag{3.4}$$

with σ_{exp} representing the experimental error and $(\sigma_{\mathrm{GP}}(\vec{x}))^2$ being the GP emulator variance.

The cost of using the GP emulators is paid in the form of running the simulation multiple times with different parameter combinations to create a set of training points for conditioning the GP. For the present investigation, we have produced 120 training points for each EoS, distributed evenly in the input parameter space using minmax Latin hypercube sampling [24]. The emulation quality was then checked by removing 20 points from the training set, conditioning the emulator on the remaining 100 and using the emulator to predict the results at the 20 excluded points. An example of the results of this confirmation process is shown in Fig. 2 for 2.76 TeV Pb+Pb collisions using the $s95p$ parametrisation.

4. Results

In this preliminary study, the chosen small subset of the available data to constrain the parameters consists of the charged particle multiplicity N_{ch} in $|\eta| < 0.5$ and 4-particle cumulant elliptic flow $v_2\{4\}$ in (10-20)%, (20-30)% and (30-40)% centrality classes. For Au+Au collisions at $\sqrt{s_{NN}} = 200$ GeV, the N_{ch} data was taken from Ref. [10] and $v_2\{4\}$ data from Ref. [9]. For Pb+Pb collisions at $\sqrt{s_{NN}} = 2.76$ TeV, the charged particle multiplicities were obtained from Ref. [11] and for $\sqrt{s_{NN}} = 5.02$ TeV from Ref. [13]. Elliptic flow data for both energies was taken from Ref. [12].

Figure 3 shows the marginal posterior distributions for each parameter (obtained from the full 5-dimensional probability distribution by integrating over the other four parameters) for the

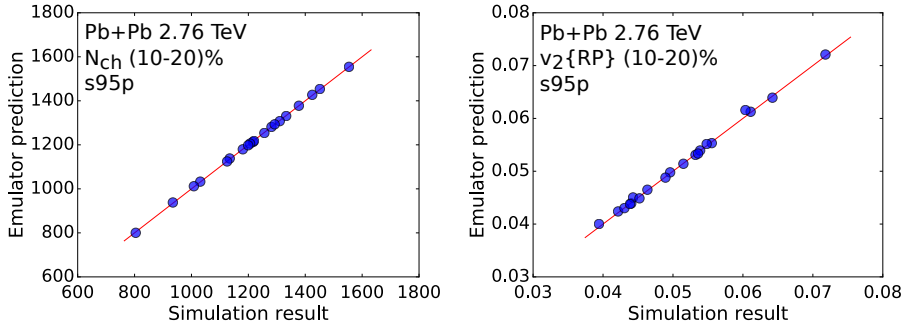

Figure 2: Illustration of the quality of the Gaussian process emulation for 20 random test points for simulations with $s95p$ equation of state. Left panel: Charged particle multiplicity in (10-20)% most central Pb+Pb collisions at $\sqrt{s_{NN}} = 2.76$ TeV. Right panel: Elliptic flow $v_2\{\mathrm{RP}\}$ in (10-20)% most central Pb+Pb collisions at $\sqrt{s_{NN}} = 2.76$ TeV.

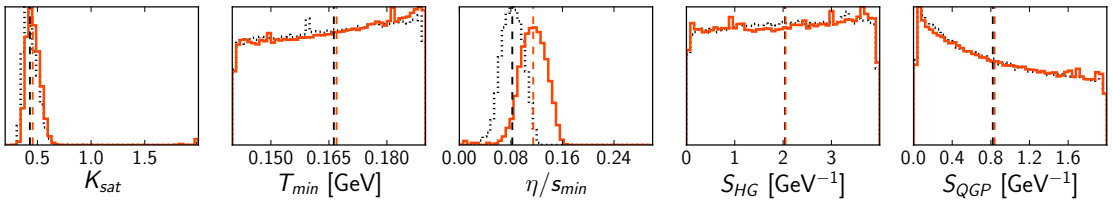

Figure 3: Marginal posterior probability distributions for EoS $s83z_{16}$ (orange solid lines) and $s95p$ (black dotted lines). Vertical dashed lines indicate the median values. The scale of the vertical axis on each panel is arbitrary.

$s83z_{16}$ and $s95p$ equations of state. Our analysis is able to find constraints for only two parameters, K_{sat} and $(\eta/s)_{min}$. For all EoSs K_{sat} peaks at 0.5, which is in agreement with the value used together with the *param1* parametrisation in Ref. [3], which in that study was found to give the best agreement with the flow coefficients. On the other hand, the peak and thus the favoured value of $(\eta/s)_{min}$ does depend on the EoS. The probability distributions of all the other parameters, T_{min}, S_{HG}, and S_{QGP}, are very flat without clear peak, which indicates that our priors, *i.e.* the intervals where parameters were allowed to vary, were too narrow and thus the median values of these distributions reflect mostly our prejudices.

We present a more detailed comparison of the most probable $(\eta/s)_{min}$ values for all four EoSs in Fig. 4. The largest difference is observed between $s95p$ and $s83z_{16}$, while the two other parametrisations $s87r$ and $s88s_{16}$ fall in-between with practically identical probability distributions. However, while the median of the distribution is sensitive to the equation of state, the 90% credibility intervals overlap even for $s83z_{16}$ and $s95p$ parametrisations. Therefore the earlier results obtained using $s95p$ parametrisation are still valid within the overall uncertainties of the fitting procedure, and it is too early to exclude the possibility that all EoSs would produce similar values for $(\eta/s)_{min}$ in a more detailed analysis.

Finally, we check how well the favoured parameter combinations reproduce the experimental data by drawing 200 samples from the posterior distribution and using the Gaussian process emu-

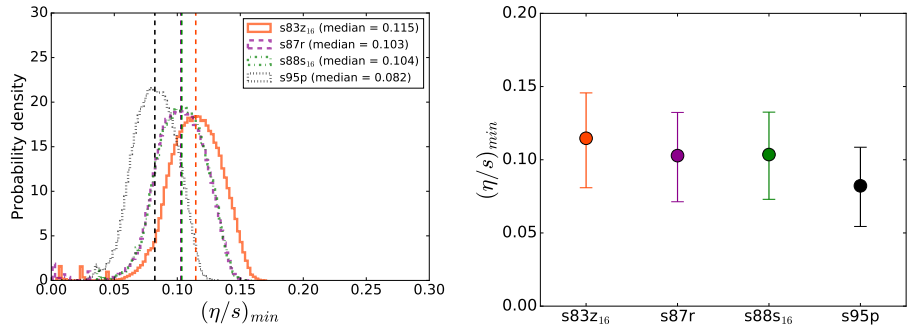

Figure 4: Comparison of $(\eta/s)_{min}$ posterior distributions for the four investigated EoSs. Left panel: Marginal probability distributions. Dashed vertical lines indicate median values. Right panel: Simplified view showing the median values (filled circles) and 90% credible intervals (error bars).

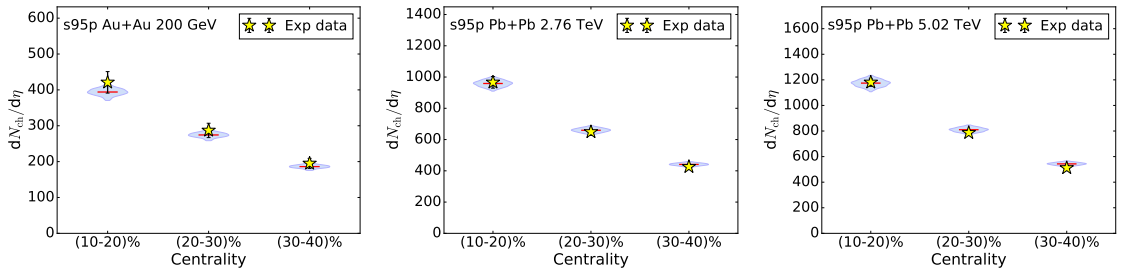

Figure 5: Predicted variation on charged particle multiplicity vs. centrality using 200 samples from the posterior distribution with the $s95p$ EoS. Wider shaded area indicates higher density of points. Horizontal lines within the shaded areas indicate the median values. Left panel: Au+Au at $\sqrt{s_{NN}} = 200$ GeV compared to STAR data [10]. Middle panel: Pb+Pb at $\sqrt{s_{NN}} = 2.76$ TeV compared to ALICE data [11]. Right panel: Pb+Pb at $\sqrt{s_{NN}} = 5.02$ TeV compared to ALICE data [13].

lator to predict the simulation output for these values. The results for charged particle multiplicities $N_{\rm ch}$ and for the elliptic flow $v_2\{4\}$ are shown in Figs. 5 and 6, respectively. The overall agreement with the data is very good for both observables over all three collision energies and centralities, assuring that the posterior distributions are indeed providing best-fit parameter values.

5. Summary

We have determined the probability distributions of the best-fit parameter values for shear viscosity over entropy density ratio η/s with a linear temperature dependence within a pQCD + saturation + hydrodynamics framework using Bayesian statistics approach. Using charged particle multiplicities and elliptic flow at three different collision energies as calibration data, we were able to find constraints for the initial state proportionality constant K_{sat} and the minimum value of shear viscosity $(\eta/s)_{min}$. While K_{sat} is found to be ≈ 0.5 regardless of the choice of the equation of state, the peak of $(\eta/s)_{min}$ distribution depends on the EoS, and the three new parametrisations $s83z_{16}$, $s87r$, and $s88s_{16}$ prefer larger values of $(\eta/s)_{min}$ compared to the baseline EoS, $s95p$. However, as the probability distributions still have a large overlap, and the parameters controlling the temperature dependence of η/s remain unconstrained, it is too early to make any strong statements about

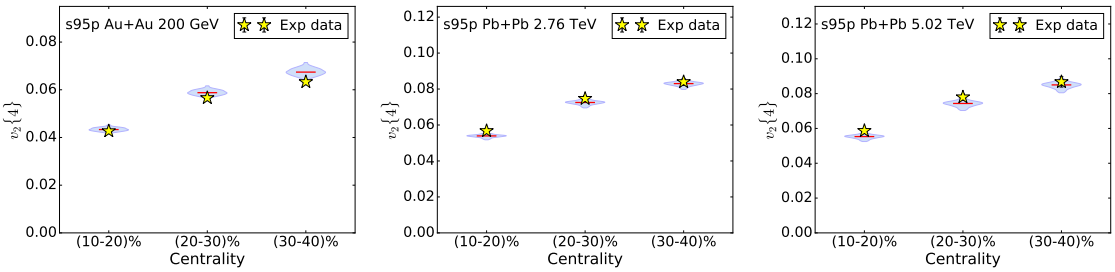

Figure 6: Predicted variation on elliptic flow vs. centrality using 200 samples from the posterior distribution with the $s95p$ EoS. Wider shaded area indicates higher density of points. Horizontal lines within the shaded areas indicate the median values. Left panel: Au+Au at $\sqrt{s_{NN}} = 200$ GeV compared to STAR data [9]. Middle panel: Pb+Pb at $\sqrt{s_{NN}} = 2.76$ TeV compared to ALICE data [12]. Right panel: Pb+Pb at $\sqrt{s_{NN}} = 5.02$ TeV compared to ALICE data [12].

the effect of EoS on the extracted shear viscosity. In Bayesian terms, better constraints are needed for both the prior (from theory) and the likelihood (from measurements).

Acknowledgements

JA was supported by the European Research Council, grant ERC-2016-COG:725741; KJE and HN were supported by the Academy of Finland, Project no. 297058; PH was supported by National Science Center, Poland, under grant Polonez DEC-2015/19/P/ST2/03333 receiving funding from the European Union's Horizon 2020 research and innovation programme under the Marie Skłodowska-Curie grant agreement No 665778; PP was supported by U.S. Department of Energy under Contract No. DE-SC0012704.

References

[1] J. E. Bernhard, J. S. Moreland, S. A. Bass, J. Liu and U. Heinz, *Applying Bayesian parameter estimation to relativistic heavy-ion collisions: simultaneous characterization of the initial state and quark-gluon plasma medium*, *Phys. Rev.* **C94** (2016) 024907 [1605.03954].

[2] S. A. Bass, J. E. Bernhard and J. S. Moreland, *Determination of Quark-Gluon-Plasma Parameters from a Global Bayesian Analysis*, *Nucl. Phys.* **A967** (2017) 67 [1704.07671].

[3] H. Niemi, K. J. Eskola and R. Paatelainen, *Event-by-event fluctuations in a perturbative QCD + saturation + hydrodynamics model: Determining QCD matter shear viscosity in ultrarelativistic heavy-ion collisions*, *Phys. Rev.* **C93** (2016) 024907 [1505.02677].

[4] S. Pratt, E. Sangaline, P. Sorensen and H. Wang, *Constraining the Eq. of State of Super-Hadronic Matter from Heavy-Ion Collisions*, *Phys. Rev. Lett.* **114** (2015) 202301 [1501.04042].

[5] J. S. Moreland and R. A. Soltz, *Hydrodynamic simulations of relativistic heavy-ion collisions with different lattice quantum chromodynamics calculations of the equation of state*, *Phys. Rev.* **C93** (2016) 044913 [1512.02189].

[6] P. Alba, V. Mantovani Sarti, J. Noronha, J. Noronha-Hostler, P. Parotto, I. Portillo Vazquez et al., *Effect of the QCD equation of state and strange hadronic resonances on multiparticle correlations in heavy ion collisions*, *Phys. Rev.* **C98** (2018) 034909 [1711.05207].

[7] P. Huovinen and P. Petreczky, *QCD Equation of State and Hadron Resonance Gas*, *Nucl. Phys.* **A837** (2010) 26 [0912.2541].

[8] A. Bazavov et al., *Equation of state and QCD transition at finite temperature*, *Phys. Rev.* **D80** (2009) 014504 [0903.4379].

[9] STAR collaboration, J. Adams et al., *Azimuthal anisotropy in Au+Au collisions at s(NN)**(1/2) = 200-GeV*, *Phys. Rev.* **C72** (2005) 014904 [nucl-ex/0409033].

[10] STAR collaboration, B. I. Abelev et al., *Systematic Measurements of Identified Particle Spectra in pp, d^+ Au and Au+Au Collisions from STAR*, *Phys. Rev.* **C79** (2009) 034909 [0808.2041].

[11] ALICE collaboration, K. Aamodt et al., *Centrality dependence of the charged-particle multiplicity density at mid-rapidity in Pb-Pb collisions at $\sqrt{s_{NN}} = 2.76$ TeV*, *Phys. Rev. Lett.* **106** (2011) 032301 [1012.1657].

[12] ALICE collaboration, J. Adam et al., *Anisotropic flow of charged particles in Pb-Pb collisions at $\sqrt{s_{\rm NN}} = 5.02$ TeV*, *Phys. Rev. Lett.* **116** (2016) 132302 [1602.01119].

[13] ALICE collaboration, J. Adam et al., *Centrality dependence of the charged-particle multiplicity density at midrapidity in Pb-Pb collisions at $\sqrt{s_{\rm NN}}$ = 5.02 TeV*, *Phys. Rev. Lett.* **116** (2016) 222302 [1512.06104].

[14] H. Niemi, K. J. Eskola, R. Paatelainen and K. Tuominen, *Predictions for 5.023 TeV Pb + Pb collisions at the CERN Large Hadron Collider*, *Phys. Rev.* **C93** (2016) 014912 [1511.04296].

[15] R. Paatelainen, K. J. Eskola, H. Holopainen and K. Tuominen, *Multiplicities and p_T spectra in ultrarelativistic heavy ion collisions from a next-to-leading order improved perturbative QCD + saturation + hydrodynamics model*, *Phys. Rev.* **C87** (2013) 044904 [1211.0461].

[16] R. Paatelainen, K. J. Eskola, H. Niemi and K. Tuominen, *Fluid dynamics with saturated minijet initial conditions in ultrarelativistic heavy-ion collisions*, *Phys. Lett.* **B731** (2014) 126 [1310.3105].

[17] Particle Data Group collaboration, S. Eidelman et al., *Review of particle physics. Particle Data Group*, *Phys. Lett.* **B592** (2004) 1.

[18] HotQCD collaboration, A. Bazavov et al., *Equation of state in (2+1)-flavor QCD*, *Phys. Rev.* **D90** (2014) 094503 [1407.6387].

[19] A. Bazavov, P. Petreczky and J. H. Weber, *Equation of State in 2+1 Flavor QCD at High Temperatures*, *Phys. Rev.* **D97** (2018) 014510 [1710.05024].

[20] Particle Data Group collaboration, C. Patrignani et al., *Review of Particle Physics*, *Chin. Phys.* **C40** (2016) 100001.

[21] S. Borsanyi, Z. Fodor, C. Hoelbling, S. D. Katz, S. Krieg and K. K. Szabo, *Full result for the QCD equation of state with 2+1 flavors*, *Phys. Lett.* **B730** (2014) 99 [1309.5258].

[22] D. Foreman-Mackey, D. W. Hogg, D. Lang and J. Goodman, *emcee: The MCMC Hammer*, *Publ. Astron. Soc. Pac.* **125** (2013) 306 [1202.3665].

[23] C. E. Rasmussen and C. K. I. Williams, *Gaussian Processes for Machine Learning*. MIT Press, Cambridge, MA, USA, 2006.

[24] "pydoe: Design of experiments for python." https://pythonhosted.org/pyDOE/randomized.html.